ELSEVIER

Journal of Nuclear Materials 313–316 (2003) 424–428

journal of nuclear materials

www.elsevier.com/locate/jnucmat

Advances in the modeling of chemical erosion/redeposition of carbon divertors and application to the JET tritium codeposition problem

J.N. Brooks [a,*], A. Kirschner [b], D.G. Whyte [c], D.N. Ruzic [d], D.A. Alman [d]

[a] *Argonne National Laboratory, 9700 S. Cass Avenue, Argonne, IL 60439, USA*
[b] *Institut fuer Plasmaphysik, Forschungzentrum Juelich, D-52425 Juelich, Germany*
[c] *University of California, San Diego, CA 92093, USA*
[d] *University of Illinois, 103 S. Goodwin Avenue, Urbana, IL 61801, USA*

Abstract

We have improved the modeling of chemically eroded carbon transport and applied this to JET and ITER. New features are: (1) coupled REDEP and ERO-JET impurity transport code calculations for sputtered wall/divertor carbon, (2) MolDyn molecular dynamics calculations of carbon/hydrocarbon particle reflection at hydrogen-saturated carbon surfaces, (3) ADAS full collisional radiative carbon ion recombination rate coefficients. At low incident particle energies relevant to chemical-erosion (~0.1–15 eV), we predict high reflection coefficients (~20–100%), implying more net erosion and T/C codeposition than for full-sticking models. Calculated tritium codeposition rates for the JET MkIIA divertor, using 'reference' chemical erosion yields of order 1% – while higher than previously estimated are well short ($X \sim 1/40$) of published data. Possible explanations include much higher chemical erosion yields.

Keywords: REDEP code; Erosion/redeposition; Carbon; Codeposition/tritium; JET; ITER

1. Introduction

Carbon remains a prime candidate surface material for a next-step fusion tokamak. It is important, therefore, to predict carbon erosion/redeposition and tritium codeposition rates, particularly for low temperature plasma regimes (detached or 'semi-detached') dominated by chemical erosion. This is one of the most difficult areas of plasma surface interactions to model. There have been recent advances in this field regarding models for chemical sputter yields, sputtered hydrocarbon species, rate coefficients for atomic and molecular processes, and other issues [1–3], but much remains to be done. In this paper we describe further key code/model improvements and application to JET and ITER carbon divertor modeling.

In particular, a critical challenge for modeling is to explain the high tritium-containing carbon deposits seen in the JET MkIIA inner divertor/wall/louver region, and to extrapolate those results to future devices. Our JET simulations do not generally match the data and show the critical need for more work, e.g., determination of chemical erosion yields of redeposited material.

2. Model improvements

2.1. Molecular dynamics calculations of carbon/hydrocarbon reflection

Previous work discussed deficiencies in models of carbon sticking/reflection and stated the need for rigor-

* Corresponding author. Tel.: +1-630 252 4830; fax: +1-930 252 3250.
E-mail address: brooks@anl.gov (J.N. Brooks).

0022-3115/03/$ - see front matter
PII: S0022-3115(02)01405-8

ous assessment [1–3]. Carbon/hydrocarbon reflection at low energies is hard to calculate with binary-collision codes, and data is sparse. Therefore, molecular dynamic calculations were performed. Reflection coefficients for low-energy carbon/hydrocarbon reflection on a hydrogen-saturated carbon surface are calculated with the MolDyn molecular dynamics code. MolDyn incorporates parameter set II of the Brenner hydrocarbon potential [4], a fixed time step third-order Beeman integrator [5], and temperature control through the velocity scaling technique of Berendsen et al. [6]. The Brenner potential was chosen because it reproduces well the covalent bonding in graphite lattices as well as in many hydrocarbon molecules. To simulate a carbon surface exposed to a hydrogen plasma, the surface was prepared from pure graphite by bombardment with 20 eV hydrogen atoms until saturation was reached. Reflection coefficients for carbon atoms and methane molecules on the resulting 0.42 H:C surface at 45° (from the normal) and 60° incidence are shown in Fig. 1. More details of the calculations and reflection coefficients of other hydrocarbon molecules analyzed are described in [7]. Work continues with this code to compute the full set of relevant hydrocarbon reflection.

Reflection data from the MolDyn code for C, CH, CH_2, CH_3, CH_4 was incorporated into the impurity transport codes with some simplifications at present (e.g., reflected hydrocarbon species = incident species only, C_2H_j reflection same as CH_j). Energy distributions of reflected particles were roughly fit to the MolDyn results using a normal distribution with mean 0.4 of the incident energy and standard deviation 0.2 of the incident energy. The reflected particle elevation angle distribution was fit with a normal distribution with mean 55° and standard deviation 20°.

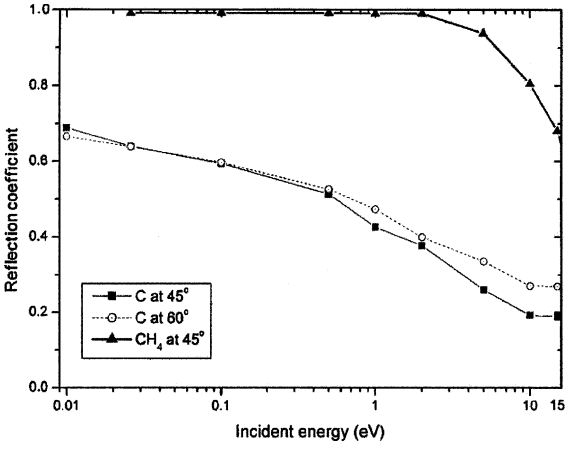

Fig. 1. MolDyn code results for the reflection coefficient of carbon and methane on a hydrogen saturated carbon surface at 45° and 60° incidence. Methane value is for total carbons reflected.

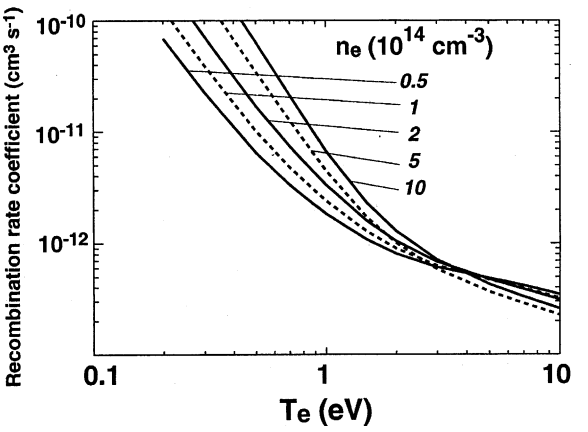

Fig. 2. Recombination rate coefficients for singly ionized carbon (C^{1+}) as a function of electron density and temperature, from ADAS [8] calculations.

2.2. Carbon ion recombination

Accurate rate coefficients for carbon ion recombination are important at very low plasma temperatures/high-density conditions. The recombination rate coefficients for singly ionized carbon (C^{1+}) are shown in Fig. 2 as a function of electron density (N_e) and temperature (T_e). The rate calculations from ADAS [8] include radiative, di-electronic, and three-body recombination. At low T_e (<2 eV) typical of detached plasmas found at inner divertor targets, one finds that three-body recombination dominates. The rate coefficient increases significantly with decreasing T_e and increases approximately linearly with n_e. The uncertainty in experimental measurement of T_e and n_e at the JET inner divertor target therefore leads to substantial uncertainty in recombination rates. However, a study of detached plasmas on DIII-D [9] with n_e and T_e measured with Thomson scattering, showed a carbon recombination rate sufficient to recombine the majority of C^{1+} ions transiting through the divertor plasma to the target.

3. JET MkIIA divertor analysis

Probably the most important PSI result in JET is the very high tritium containing carbon deposits found in the inner divertor louver region for an integrated campaign of about 10 000 s of plasma operation with the JET MkIIA divertor. This amount of carbon has been estimated experimentally to be ~4% of the total number of incoming deuterium ions Φ_{D+} to the inner divertor region [10]. Studies [1–3,10,11] analyze various aspects

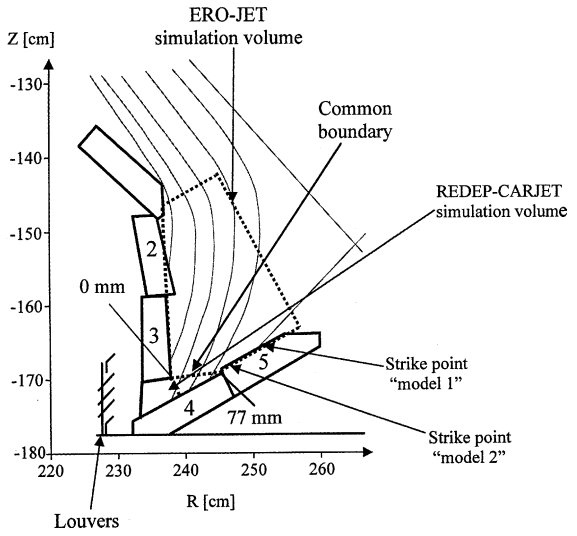

Fig. 3. JET MkIIA inner divertor geometry and calculation set-up.

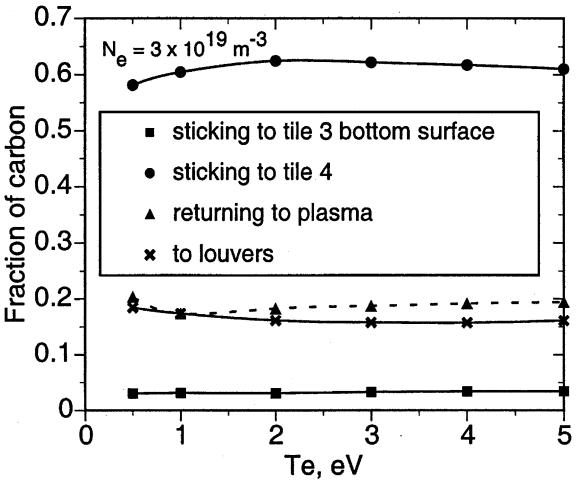

Fig. 4. Fate of 100 000 carbon atoms and ions entering the REDEP/CARJET simulation volume along the common boundary. Boundary conditions given by ERO-JET results. As a function of plasma electron temperature in CARJET volume, for the fixed density shown.

of this problem. We have now coupled ERO-JET (subset of ERO-TEXTOR [12] code) and REDEP/CARJET (part of REDEP/WBC [13] code package with specialized geometry for the JET problem) calculations, all using the updated reflection and recombination models, and previous upgraded atomic and molecular process models. (Assumptions/models used in these codes are reasonably consistent but not fully so.)

Fig. 3 shows the volumes used for the coupling of these codes where the 7.7 cm wide common boundary (dotted line) is shown. Along this boundary ERO-JET provides the following information which is used as input for the CARJET calculations: amount and spatial distribution of hydrocarbons and carbon, distribution of the charge state of the species, and their mean energy. This is determined by wall and divertor chemical erosion, including drifting carbon background from the entire machine. Due to experimental uncertainties, two strike point locations 8 cm apart are modeled. (An additional strike point on tile 3 was not modeled due to lack of plasma data, but it is believed that the carbon transport should be reasonably similar to the cases analyzed.) Details of the ERO-JET calculations are given in [11].

Below the common boundary CARJET computes the transport of entering carbon/hydrocarbon to each surface shown, including material returning to the plasma. In addition, the WBC code computes the fate of all hydrocarbons sputtered from the tile 4 surface. Because the JET plasma in this region is not well characterized, we parametrized the plasma temperature and density over broad ranges, with a nominal reference of 3 eV, 3×10^{19} m^{-3}.

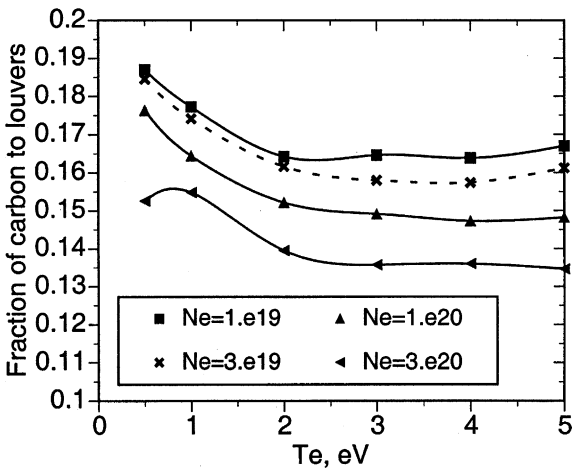

Fig. 5. CARJET computed carbon fraction to the louvers as a function of CARJET-volume electron temperature (T_e) and electron density (N_e).

Figs. 4 and 5 show selected CARJET results, averaged equally over the two strike point locations. Carbon goes to the louvers via two main processes: (1) plasma volume recombination of entering ions and subsequent line-of-sight transport of the carbon atoms, (2) reflection of ions or atoms from the tile 4 surface directly to the louvers or via further reflection from the tile 3 surface. Weaker processes include diffusion of ions across field lines into the louver region. Although variations in the carbon transport fractions with plasma parameters are

not large, with louver fractions varying from about 15–20%, there are major differences in the physical processes, with recombination/carbon-atom transport dominating at low T_e, high N_e, and initial ion transport to the tile 4 surface dominating otherwise. In general, louver fractions decrease with increasing T_e due to lower sticking at the higher energies, and louver fractions decrease with increasing N_e due to higher recombination and subsequent higher atom back-flux to the plasma.

The second source of carbon to the louvers is chemical sputtering of the tile 4 surface. The WBC calculations (not shown) of the transport of chemically eroded hydrocarbons from tile 4 show about ~20% of tile 4 sputtered material going to the louvers for the reference plasma conditions. (This is thus a similar louver fraction as the material entering the CARJET volume, but there are more variations with plasma parameters.) Due to relatively low D^+ fluxes to tile 4 – under most assumed plasma conditions – the chemical erosion of tile 4 appears to contribute less to carbon louver flow than does erosion of the rest of the divertor/wall.

Based on the combined code analysis and using the key parameter of the chemical erosion yield Y_{chem} (total carbon emitted per incident deuterium atom or ion), we can compare the code predictions for louver carbon to the JET data. The amounts simulated include:

- 0.076% Φ_{D+} for $Y_{chem} = 1\%$, model 1 strike point.
- 0.13% Φ_{D+} for $Y_{chem} = 1\%$, model 2 strike point.
- 1.3% Φ_{D+} for $Y_{chem} = 10\%$, model 2 strike point.

These are lower than the data by factors of about 30–50 for the 1% yield cases and vary linearly with Y_{chem}. The lower yield is in the range generally recommended for ITER calculations [14,15] based on models and data for low energy D impact on pyrolytic graphite. Data exists indicating that hydrogenated redeposited net-growth carbon may suffer much higher (~10–25) erosion yields [16]. As discussed more fully in [10,11,17] such material is apparently present on the JET inner wall region due to sputtering and transport of carbon from the rest of the wall and from the outer divertor. The higher-yield theory is partially consistent with the present results, i.e., it tends to explain the high louver deposits but not the divertor erosion pattern, although more analysis is needed, e.g., to examine variable yield effects on the erosion profile.

Several other model variations/effects were considered in an attempt to better reproduce the data including sputtering by much higher D^0 fluxes and thermal desorption of divertor material by ELM heating. Evidence for these other effects does not appear compelling but more assessment is needed.

Other code/data comparisons, in particular for carbon and tritium deposits on the non-louver surfaces need further assessment, but these are more difficult than the louver comparison, due to the lack of key data.

4. ITER analysis

The WBC code with the upgraded reflection and recombination models was used to predict tritium codeposition in the current ITER-FEAT carbon target divertor design, with semi-detached plasma. Details are discussed in [18]. The main prediction is a codeposition rate of ~7 mg T/s, based on the ~1–2% 'subcommittee model' Y_{chem} range [14]. The peak gross and net erosion rates are ~115 and 20 nm/s. Obviously, in view of the JET results this must be regarded as highly uncertain. ITER however, does not have a carbon wall, has a non-shadowed (see below) divertor geometry, and will run much hotter – these factors should all tend to reduce erosion/codeposition compared to JET.

5. Discussion

A previous examination of the deuterium deposition patterns in DIII-D, JET (MkI), and ASDEX-Upgrade tokamaks [19] showed a similar global trend in codeposition to the JET MkIIA results under consideration here. Namely, the inner divertor region is the predominant location of deposition, and the rate of codeposition is large (~$0.5–1 \times 10^{20}$ C m^{-2} s^{-1} average net carbon deposition rate or ~1% of incident ion flux). However, those carbon deposits were found mostly on plasma-facing surfaces, in contrast to the JET MkIIA results with deposition at the louver region recessed from the plasma-facing surfaces. Unlike the JET MkIIA campaign, all the divertor configurations of [19] were closed; that is, there were no significant openings with access to cold surfaces.

Another unique aspect of the JET divertor design is the intentional tilting of the divertor tiles in the toroidal direction in order to avoid leading edge heating. This leads to some toroidal portion of each tile being shielded or shadowed from direct SOL plasma contact. In the MkI closed case (no louvers) the C and D deposits were predominately (~70–80%) found in these shadowed regions. Considering the shadowed region to be the 'natural' location of deposits, we speculate that carbon erosion/transport from these regions, which experience high D atom flux through charge-exchange and 'see' the louvers, is important. Qualitatively, we expect longer dissociation and ionization mean-free-paths for hydrocarbon volatiles and radicals in the weak plasma directly contacting these shadowed region and, therefore, more efficient transfer of HC to the louver region. However, to date this specific three-dimensional nature of the C/D deposition has not been modeled.

6. Conclusions

Combining our previous work with modeling atomic and molecular processes of the emitted and plasma-generated hydrocarbon species, and with the addition of the here-described reflection and recombination calculations, we have eliminated essentially all 'free parameters' from the impurity transport calculations for chemically sputtered carbon – given a specific plasma solution. The one major exception is the chemical erosion yield.

From the JET code/data discrepancies it is clear that a good deal of additional modeling and experimental work is still needed to obtain predictive capability for carbon surfaces operating with detached plasmas. Likewise, although erosion and tritium codeposition estimates for ITER FEAT are marginally acceptable, this is subject to considerable uncertainties in carbon erosion/transport for the semi-detached plasma regime chosen to minimize divertor heat load. This contrasts to the generally good code/data comparisons obtained for carbon physical sputtering in non-detached plasmas, e.g. for DIII-D experiments [20]. Work to reduce uncertainties should include well-diagnosed in situ tokamak experiments with eroded-redeposited carbon, transport of eroded and injected hydrocarbons, and associated modeling.

Acknowledgements

US work supported by the US Department of Energy, Office of Fusion Energy.

References

[1] J.N. Brooks, D.A. Alman, G. Federici, D.N. Ruzic, D.G. Whyte, J. Nucl. Mater. 266–269 (1999) 58.
[2] D.A. Alman, D.N. Ruzic, J.N. Brooks, Phys. Plasmas 7 (2000) 1421.
[3] A. Kirschner et al., Phys. Scr. T81 (2001) 57.
[4] D.W. Brenner, Phys. Rev. B 42 (1990) 9458.
[5] D. Beeman, J. Comp. Phys. 20 (1976) 130.
[6] H.J.C. Berendsen, J.P.M. Postma, W.F. van Gunsteren, A. DiNola, J.R. Haak, J. Chem. Phys. 81 (1984) 3684.
[7] D.A. Alman, D.N. Ruzic, these Proceedings.
[8] H. Summers, Atomic Data and Analysis Structure-User Manual, Abingdon, UK, JET-IR (94) 1994.
[9] D. Whyte et al., Nucl. Fusion 41 (2001) 1243.
[10] J.P. Coad et al., J. Nucl. Mater. 290–293 (2001) 224.
[11] A. Kirschner et al., Hydrocarbon transport in the MkIIa divertor of JET, Plasma Phys. Control. Fusion, in press.
[12] A. Kirschner, V. Philipps, J. Winter, U. Kögler, Nucl. Fusion 40 (5) (2000) 989.
[13] J.N. Brooks, Nucl. Tech. Fusion 4 (1983) 33;
Fus. Tech. 18 (1990) 239;
Phys. Fluids 8 (1990) 1858;
Fus. Eng. Des. 60 (2002) 515.
[14] G. Federici et al., J. Nucl. Mater. 266–269 (1999) 14.
[15] J. Roth, J. Nucl. Mater. 266–269 (1999) 51.
[16] E. Vietzke, A.A. Haasz, in: W.O. Hofer, J. Roth (Eds.), Physical Processes of the Interaction of Fusion Plasmas with Solids, Academic Press, San Diego, 1996, p. 135.
[17] J.P. Coad et al., these Proceedings.
[18] G. Federici et al., these Proceedings.
[19] D.G. Whyte, J.P. Coad, P. Franzen, H. Maier, Nucl. Fusion 39 (1999) 1025.
[20] J.N. Brooks, D.G. Whyte, Nucl. Fusion 39 (1999) 525.